Pain. Author manuscript; available in PMC 2016 July 05.

Published in final edited form as:
Pain. 2015 November ; 156(11): 2267–2275. doi:10.1097/j.pain.0000000000000299.

Striatal opioid receptor availability is related to acute and chronic pain perception in arthritis: Does opioid adaptation increase resilience to chronic pain?

Christopher A Brown[1], **Julian Matthews**[2], **Michael Fairclough**[2], **Adam McMahon**[2], **Elizabeth Barnett**[2], **Ali Al-Kaysi**[3], **Wael El-Deredy**[4], and **Anthony KP Jones**[5]

[1]CamPAIN group, Department of Anaesthesia, University of Cambridge, Cambridge, United Kingdom, CB2 0QQ

[2]Wolfson Molecular Imaging Centre, University of Manchester, Manchester, United Kingdom, M20 3LJ

[3]Department of Anaesthesia, Southport and Ormskirk Hospitals, Southport, Merseyside, United Kingdom, PR8 6PN

[4]School of Psychological Sciences, University of Manchester, Manchester, United Kingdom, M13 9PL; School of Biomedical Engineering, University of Valparaiso, Chile

[5]Human Pain Research Group, Institute of Brain, Behaviour and Mental Health, University of Manchester, Salford, United Kingdom, M6 8HD

Introduction

Chronic pain is frequently reported by patients with arthritis [58]. However, there is no correlation between pain and structural joint damage in osteoarthritis [5]. The basis of variability between pathophysiology and pain outcomes is unknown. One possibility is natural variability in pain regulation within the central nervous system (CNS).

The ascending spinothalamic pathways that mediate nociception terminate in multiple thalamic nuclei and cortical brain regions [20]. Cortical sites modulate nociception partly by projecting to the basal ganglia including the striatum, which also receives afferent nociceptive inputs from the spinal cord via the globus pallidus [6]. Striatal nuclei, including the caudate, putamen and nucleus accumbens, are the most densely populated regions for opioid receptors in the brain [4,14,34], and are thought to be important for opioid-mediated endogenous analgesia [12,21]. The possibility of opioid mechanisms being involved in determining individual differences in pain states has been a key topic of recent research [28,41,60], but the functional consequences of chronic pain on OpR physiology are largely unknown.

Correspondence to: Dr Christopher A Brown, CamPain group, Division of Anaesthesia, Box 93, Addenbrooke's Hospital, Cambridge, CB2 0QQ, cb802@cam.ac.uk.

The authors declare no competing financial interests.

Europe PMC Funders Author Manuscripts

It has long been known that prolonged nociception results in the release of endogenous opioid peptides and subsequent agonism of OpRs in the CNS [19]. However, a relatively unexplored hypothesis is that chronic pain could potentially adjust OpR physiology to provide more efficient dampening of the pain response as part of a homeostatic control mechanism. There is evidence from animal studies that delta and kappa-OpRs, found in the brain and spinal cord [8,11], can be up-regulated in response to mu-OpR agonism [56], thereby increasing the anti-nociceptive potency of delta-OpR agonists [38,44]. Animal models of chronic inflammatory pain have shown an increase in cell membrane expression of delta-OpRs both postsynaptically [9] and presynaptically [22] in the dorsal spinal cord ipsilateral to the site of injury. Stimulus-evoked translocation of delta-OpRs to neuronal plasma membranes may have evolved as part of a homeostatic mechanism to maintain control of nociceptive transmission [7]. However, evidence for such a mechanism in humans is lacking.

Positron Emission Tomography (PET) receptor binding studies enable assessment of the endogenous opioid system in humans via radiotracers that bind to opioid receptors (OpRs), such as carbon-11 labelled diprenorphine ([^{11}C]-DPN), an antagonist that binds equally well to mu, delta and kappa OpRs [31,33]. Here we measured OpR availability in patients with arthritis and healthy controls with [^{11}C]-DPN PET imaging, to identify relationships between OpR availability and the level of perceived acute and chronic pain. Our analysis revealed associations between the striatum and the perception of both acute and chronic pain. We interpret our findings in relation to the hypothesis, supported by the aforementioned evidence from the animal literature, of adaptive upregulation of OpR binding sites in chronic pain states.

Materials and Methods

The research study was approved by Stockport NHS Research Ethics Committee (reference 09/H1012/44) and permission granted by ARSAC (radiation protection agency).

Participants

17 patients (12 females) and nine healthy control participants (3 females) were recruited into the study. All participants gave written informed consent. The characteristics of the participants are shown in Table 1. Patients were recruited from primary and secondary care in Greater Manchester, while healthy control participants were recruited from an existing database of research volunteers, and from primary care in Greater Manchester. 15 participants had a diagnosis of Osteoarthritis (OA) while 2 had a diagnosis of Rheumatoid Arthritis (RA). All patients had experienced chronic pain for at least the past three months. OA and RA patients fulfilled the American College of Rheumatology (ACR) criteria for the diagnosis of OA [3] and RA [1]. No control participants were experiencing any chronic pain or other recurrent health problems. Exclusion criteria for both groups included age of <35 years, and medical records showing a history of neurological disorder, morbid psychiatric disorder (including major depression and anxiety-related disorders confirmed by a psychiatrist), organ failure or cardiovascular disease. It was expected that patients would be

recruited with sub-clinical levels of anxiety and depression that are normal for chronic pain populations.

Any patients taking opioid analgesic medication, of which there were two, were asked to withdraw prior to scanning. The timing of this withdrawal was determined on a case-by-case basis, but was started no more than 2 weeks prior, and completed not later than 2 days prior, to each scanning session. Any paracetamol or NSAIDs were withdrawn at least 24 hrs prior to scanning.

MRI data acquisition and pre-processing

A T_1-weighted MRI brain scan was acquired for the purpose of excluding structural abnormality, co-registration and spatial normalization of PET images (see Supplementary Methods). MRIs were segmented into white matter, grey matter and cerebrospinal fluid using Statistical Parametric Mapping (SPM8, Wellcome Department of Imaging Neuroscience, Institute of Neurology, UCL, London, UK) running on Matlab version 7.10 (The Mathworks Inc., Natick, MA, USA).

Questionnaire assessments

Patients (but not healthy controls) completed an assessment of clinical pain as experienced over the last week, prior to PET scanning. Clinical pain was measured using the short-form McGill Pain Questionnaire (MPQ) [42], which has subscales for sensory and affective pain.

Positron Emission Tomography (PET) scans

A cannula was inserted into a radial artery of the non-dominant forearm after a satisfactory modified Allen's test and local anaesthesia, for sampling of arterial blood during the scan. An intra-venous cannula was inserted into the dominant forearm for radiotracer injection.

Patients were scanned using a Siemens/CTI High Resolution Research Tomograph (HRRT; CTI/Siemens Molecular Imaging, TN, USA [35]) PET scanner at the Wolfson Molecular Imaging Centre, capable of 2.5 mm resolution. Participants were positioned supine with their transaxial planes parallel to the line intersecting anterior and posterior commissure (AC–PC line). Head position was measured and equated as best as possible in both PET sessions. Head movement during scanning was discouraged by applying gentle pressure to the nasion via a padded attachment to the head holder. Patients wore a customized neoprene cap with a reflective tool attached to the vertex that was used to continuously assess head motion using a Polaris Vicra infrared motion detector (Northern Digital, Ontario, Canada). Prior to further scanning, a 6 min transmission scan was performed for attenuation correction, facilitated by a ^{137}Cs transmission point source [36].

Regional cerebral blood flow (rCBF) was measured to allow for assessment of the relationship of [^{11}C]-DPN binding results to rCBF. Following the transmission scan and immediately prior to the [^{11}C]-DPN scan, 510 MBq to 645 MBq (target dose: 600MBq) of ^{15}O-labelled water ($H_2{}^{15}O$) was administered, using an automatic radio water generator (HIDEX Inc., Turku, Finland) (see Supplementary Methods). This was followed by an i.v. smooth bolus subpharmacological tracer dose of [^{11}C]-DPN injected over 20 s, followed by

a 20 s saline flush. [^{11}C]-DPN was initially synthesized in situ at the Wolfson Molecular Imaging Centre using the methylation method [18]. Characteristics of [^{11}C]-DPN doses are shown in Supplementary Table 1. A 90-minute continuous acquisition in list mode followed injection (see Supplementary Methods).

For both the [^{11}C]-DPN and $H_2{}^{15}O$ scans, continuous measurements of the radioactivity in arterial blood were conducted, as well as further intermittent discrete arterial blood sampling took place for cross-calibration and to determine the partition of blood radioactivity between plasma and whole blood (erythrocytes) (see Supplementary Methods).

Derivation of arterial input function

The input function of parent [^{11}C]-DPN in arterial blood plasma was derived as follows. To obtain the time-course of whole blood radioactivity over time, the continuous blood data from the first 10 min of the [^{11}C]-DPN scan was firstly calibrated against radioactivity measured in discrete blood samples (via a well counter) at corresponding time points. This initial time-course was then spliced with an interpolation of the discrete blood radioactivity data over the remainder of the scan to obtain the full time-course. From the discrete blood samples, the plasma-over-blood ratio was calculated and linearly fitted. Using the radio-HPLC data, the percentage of radioactivity attributed to the parent radiotracer in plasma was fitted as an exponential function in which time zero was restricted to unity. Input functions were then derived by multiplying (a) the time course of radioactivity in whole blood, (b) the linear function describing the plasma-over-blood ratio over time, and (c) the exponential function describing the parent fraction in plasma over time.

[^{11}C]-DPN and $H_2{}^{15}O$ PET image reconstruction

PET images were reconstructed to a 256 × 256 × 207 matrix (isotropic voxel size of 1.21875 mm^3) using an iterative Ordinary Poisson Ordered Subset Expectation Maximization algorithm (OP-OSEM; 12 iterations). The reconstruction was performed using the HRRT user community software with the default resolution kernel [13]. Following reconstruction, the dynamic images were trimmed, calibrated and stored as Analyze 7.5 formatted images. The calibration factor was determined using a uniform head-sized phantom which is scanned periodically (˜every 2 weeks).

Derivation of ^{11}C-DPN Volume of Distribution (VD_{DPN}) and $K1_{DPN}$

Parametric images of the [^{11}C]-DPN volume-of-distribution (VD_{DPN}) and the [^{11}C]-DPN rate of uptake from blood to tissue ($K1_{DPN}$) were calculated using spectral analysis [55] and implemented using the non-negative least squared algorithm (conventional spectral analysis [15]). Inputs to this analysis were the dynamic PET images and the arterial input function, both uncorrected for decay of ^{11}C. The fast frequency boundary was set to 0.02 s−1 and the slow frequency boundary to 0.0008 s−1. The slow frequency boundary was informed by two considerations: (a) the slowest possible kinetics of [^{11}C]-DPN, which is limited by the physical decay constant of the isotope (0.0005663 s−1), deriving from the half-life of ^{11}C (20.4 min), (b) data evaluating the image quality, reproducibility and reliability of [^{11}C]-DPN VD images across a range of slow frequency boundaries, which identified 0.0008 s−1 as being superior to lower cut-offs that were closer to the decay constant of ^{11}C [27]. The

spectra were spaced logarithmically and the magnitude normalised so that the weighted columns summed to unity. Individual data points were weighted according to the reciprocal of the variance, as estimated from the frame duration over the total image concentration. A delay, which was fixed over the entire image volume, was estimated by fitting the same spectral analysis model to a TAC from a ROI over the entire image volume and varying the delay using a golden line search algorithm to determine the delay that minimised the weighted least squared error.

Derivation of regional cerebral blood flow (rCBF)

Parametric images of the $H_2{}^{15}O$ kinetic parameter $K1_{H2O}$ (ml min-1 ml-1), a measure of rCBF, were obtained using a one-tissue compartment model in which $K1_{H2O}$ is the rate of uptake of $H_2{}^{15}O$ from blood to brain. An input function of total radioactivity in whole blood was used that was calculated by scaling the continuous blood data, as with the [^{11}C]-DPN blood data. Reconstructed $H_2{}^{15}O$ PET images were initially smoothed with a 4mm FWHM Gaussian kernel prior to kinetic modeling using the Generalized Linear Least Squares (GLLS) algorithm.

VD_{DPN}, $K1_{DPN}$ and $K1_{H2O}$ image pre-processing

Pre-processing of parametric images was performed using SPM8 (Statistical Parametric Mapping, Wellcome Department of Cognitive Neurology, London, UK). Each PET image were co-registered onto the corresponding T1-weighted MRI image using rigid-body transformation derived from the normalized mutual information measure of image matching [40]. Next, MRI images were spatially normalised into the International Consortium for Brain Mapping (ICBM) standardized space (Montreal Neurological Institute, Montreal, Canada) using nonlinear basis functions, with the same transformation characteristics then applied to the co-registered parametric PET images.

Calculation of global $K1_{DPN}$

Kinetic modelling of [^{11}C]-DPN using spectral analysis is based on a compartmental model in which delivery of the radiotracer (represented by the parameter $K1_{DPN}$) to brain tissues is modelled separately to specific binding (represented by VD_{DPN}) and non-specific binding (to other cellular molecules). However, $K1_{DPN}$ would be expected to change along with blood flow as a result of differences in pain state. In particular, delivery effects may act as a confounder of the positive relationship between chronic pain perception and radiotracer binding: it would be expected that chronic pain would increase blood flow to the brain and increase the concentration of radiotracer in regions of interest. We controlled for radiotracer delivery effects within the statistical analysis by removing any variance in VD_{DPN} that could be accounted for by global $K1_{DPN}$ (the parameter estimating radiotracer delivery). While a reliance on global values of $K1_{DPN}$ might not be ideal we determined that *regional* $K1_{DPN}$ did not correlate with regional VD_{DPN} as a result. The weighted average of $K1_{DPN}$ values in grey matter across the whole brain were therefore calculated for each scan. $K1_{DPN}$ values in grey matter were initially identified using a grey matter mask on $K1_{DPN}$ images.

Analysis of head motion data

Head motion is a nuisance variable that could potentially cause unwanted between-subject and/or between-group variability in VD_{DPN} values. We therefore controlled for head motion in statistical tests. Quantitative head motion data was collected from the Vicra system, but the raw data was considered unreliable due to the observation that the head was able to move to a small extent within the neoprene cap worn by the participant to mount the head motion sensors. Analysis of head motion data was therefore performed in semi-quantitative manner, in that it relied on some qualitative assessment to achieve an ordinal score of total motion.

Head motion data consisted of both translational and rotational movements, each represented by three separate time-courses for each dimension of movement. Using visual inspection of this data, each [^{11}C]-DPN scan was scored separately for (a) intra-scan motion taking place over two or more dynamic frames of the PET data, (b) motion taking place between the transmission scan and the [^{11}C]-DPN scan, (c) the magnitude of infrequent intra-frame discrete motion events (d) the magnitude of frequent intra-frame motion events (Supplementary Table 2). Separate scales were used to score each item for the degree of motion observed to account for the likely impact of that motion on the quality of the PET data. Movements of less than 1 mm translation, or 1 degree of rotation (which roughly equates to a 1 mm movement of superficial cortical regions), were considered inconsequential due to the resolution of the PET camera at 2.5 mm. Intra-frame motion events were scored higher (and higher again with greater frequency) than motion events spanning across two or more dynamic frames of PET data, because the latter were at least partially corrected during reconstruction. Scores for each type of motion were summed to create an overall motion severity score for each scan. Two researchers scored the head motion data independently and these scores were meaned.

Assessment of acute thermal pain threshold

The order of PET and thermal pain threshold assessments were randomised between participants and occurred on different days within four weeks of each other. Acute pain was induced using a CO_2 laser (150ms duration, beam diameter of 15mm), which specifically activates nociceptors in the skin [43], applied to the dorsal surface of the subjects' right forearm. Between stimuli, the laser was moved randomly over an area 3cm x 5cm to avoid habituation, sensitization or skin damage, with stimuli occurring at 10 s intervals. Subjects wore protective laser safety goggles.

To determine pain threshold, the Method of Levels was used. Participants were instructed to attend to the intensity of each laser stimulus and to rate it using a 0-10 numerical rating scale (NRS), which was anchored such that a level 4 indicated pain threshold, 7 indicated moderate pain, and 10 indicated unbearable pain. Laser stimuli were gradually increased in steps of 0.3 W cm-2 stimulus irradiance, from zero up to a subjective intensity of 7/10, and repeated three times. Pain threshold was considered as the mean stimulus energy, over the first three ramps, required to elicit a response of 4/10.

Europe PMC Funders Author Manuscripts

Statistical analyses

Statistical analyses were conducted on [^{11}C]-DPN VD images on a voxel-by-voxel basis across the whole brain using SPM8 software. Before whole-brain analyses, smoothing of images was performed using a three-dimensional Gaussian kernel of 8 mm.

Whole-brain regression analyses were conducted within the patient group ($n = 17$) to identify regions correlating with sensory and affective dimensions of pain (Short-Form McGill Pain Questionnaire, sensory and affective subscales). In all tests, a number of covariates controlled for nuisance variables: subjects' age (years), subjects' sex (binary), subjects' weight (kg), [^{11}C]-DPN dose injected (MBq), global $K1_{DPN}$ (min^{-1}), head motion scores, and mean NRS ratings of pain reported across the whole scan. For all whole-brain comparisons, results are reported at uncorrected probability thresholds of $p < 0.001$ with a minimum cluster size of 50 voxels, and results are considered statistically significant after voxel-level correction for multiple comparisons using the Family-Wise Error rate set to 0.05.

Further analyses were conducted on regions-of-interest (ROIs) whose values were obtained as follows. From each scan, VD_{DPN} values were extracted from ROIs in which supra-threshold clusters (after FWE correction) were found. Most ROIs were defined by anatomical labels within a previously published probabilistic atlas of the human brain [26], except for the periaqueductal gray (PAG) whose ROI was constructed from three overlapping 6-mm spheres along the central aqueduct (in mm [0 −24 −4; 0 −26 −6; 0 −29 −8]) as done in previous work [48]. A weighted average of VD_{DPN} values within ROIs was calculated. $K1_{DPN}$ and $K1_{H2O}$ values were obtained from ROIs in the same way.

ROI analyses sought to identify group differences and correlations with pain threshold. Firstly, ROIs from the patient (n = 17) and healthy control (n = 9) groups were statistically compared using an independent samples t-test with significance threshold of $p < 0.05$, after corrections had been made to the mean VD_{DPN} within each ROI by controlling for variance related to nuisance variables. The same nuisance variables were used as in the whole-brain analysis described above. Secondly, ROI data from each group separately, and also from the pooled data across both groups, were correlated with pain threshold as assessed by the acute laser stimuli. Mean ROI values were first corrected for nuisance variables as described above, with an additional variable being each subjects' 0 – 10 NRS rating of acute laser pain intensity. Pearson's produce-moment correlation coefficient was obtained and results were considered statistically significant at $p < 0.05$.

To test for whether rCBF explained any of the variances in the VD_{DPN} data after correction for $K1_{DPN}$, mean $K1_{H2O}$ within ROIs were tested for correlation with both mean VD_{DPN} within the same ROIs, and predictor variables of interest showing statistically significant relationships with VD_{DPN} (namely, McGill sensory and affective pain scores and acute pain threshold). $K1_{H2O}$ for the patient (n = 14) and control (n = 8) groups were also compared by independent samples t-test in the same way as for the VD_{DPN} data.

Results

Participant characteristics and group comparisons

Data for group comparisons of sex, age, weight, radiotracer doses, intra-scan pain ratings, head motion during scanning and acute laser thermal pain thresholds are shown in Table 1. There was a larger proportion of females in the patient group (that was not statistically significant), and patients were significantly older than healthy controls. The dose of [^{11}C]-DPN injected, and the weight of participants (which may impact on radiotracer concentrations reaching the brain) did not significantly differ between groups, while the dose of water injected to assess rCBF was overall greater in patients than controls. On average, patients reported being in greater pain than controls during scanning, but the results were not statistically significant suggesting that efforts to make patients comfortable were at least partially successful. However, patients on average showed more than twice as much head motion during scanning, although this did not reach statistical significance compared to the healthy group. Lastly, while patients may scale pain differently due to their prior experience of chronic pain, we found no evidence of a difference in pain thresholds between groups.

Effect of chronic pain perception on opioid receptor availability

Whole-brain SPM regression analysis (Figure 1a and 1b, Supplementary Table 3) revealed that in chronic pain patients, McGill sensory pain scores, for their chronic pain over the previous week, was significantly and positively correlated with opioid receptor availability at the cluster level in the caudate nucleus, continuous with the nucleus accumbens and the subcallosal area. The right mid-insula showed the same effect at just below the level of significance. As the data were corrected for head motion in this statistical model, the greater VD values could not be ascribed to this factor. Also, having corrected for delivery effects in the analysis using the kinetic parameter K1, the mean VD values were not correlated with rCBF in the caudate ($r = 0.27$, $p = 0.35$), nor was rCBF related to chronic pain perception (Table 2), suggesting that the relationship between chronic pain perception and VD in the region of interest was not driven by greater blood flow in patients experiencing greater chronic pain.

As confirmation that the main result in the caudate was not related to modification of the endogenous opioid system by recent use of opioid medication, ROI analysis on the whole caudate was found to be comparable for the whole patient group ($n = 17$, $r = 0.691$, $p = 0.002$) and for a restricted patient group that excluded those withdrawn from opioid medication for the purpose of scanning ($n = 15$, $r = 0.687$, $p = 0.005$).

Analysis on a further ROIs (putamen, insula, thalamus and PAG, Table 2), in which mean VD values were taken over each ROI bilaterally, also revealed significant associations between chronic pain perception and opioid receptor availability, suggesting a broad relationship between chronic pain and opioid receptors availability across a network of brain regions expressing opioid receptors, including those involved with descending inhibition of nociception. Testing the same ROIs against patients' affective pain perception (McGill affective pain scores) yielded a significant positive relationship within the caudate nucleus and subcallosal area only.

Opioid receptor availability correlation with pain threshold

Opioid receptor availability was found to be positively correlated with laser heat pain threshold in both the caudate and subcallosal area (Table 2), with the strongest effect in the caudate (Figure 1c). Effects were close to significance in the putamen and insula, but not in nucleus accumbens. The strength of the effect was also greater (for caudate and the subcallosal area) in the pooled data over both groups, with individual groups showing weaker relationships (leading to effects above the threshold of significance in the subcallosal area) consistent with the fewer degrees of freedom when considering individual groups.

Pain thresholds were also related to rCBF in the caudate nucleus, but on further assessment rCBF was not related to diprenorphine VD values in the caudate ($r = 0.21$, $p = 0.36$), and so the relationship between the OpR binding and rCBF results remain obscure.

Group differences in opioid receptor availability

Group comparison of mean VD values in ROIs revealed overall lower opioid receptor availability in the caudate nucleus in patients relative to controls (Table 2). While opioid receptor availability was also lower in patients in the subcallosal area and nucleus accumbens, these effects did not reach significance. There were no group differences in any other ROIs, suggesting that these results are specific to the ventral striatum. There were no group differences in rCBF in the caudate nucleus.

Discussion

Three key findings emerge from this study: Firstly, that the perception of higher levels of chronic pain within the arthritis group was related to greater OpR availability across pain modulatory regions of the basal ganglia, insula and PAG, and particularly strongly within the caudate, nucleus accumbens and subcallosal area. This is the first time this has been reported in patients with arthritic pain. The result is consistent with the hypothesis of upregulation of receptor sites in those experiencing greater chronic pain, although the hypothesis itself is not directly tested here. Secondly, OpR availability in the caudate was positively associated with acute thermal pain threshold (in both patients and controls), supporting the view that upregulation of OpRs in the striatum is adaptive in acting to dampen pain perception. Thirdly, overall caudate OpR availability was reduced in arthritis patients relative to healthy controls, consistent with greater release of endogenous opioid peptides and consequent occupation of OpR binding sites in the arthritis group. Our analyses were strengthened by controlling for radiotracer delivery effects and head motion, two factors that are likely to be both responsive to pain states and have an influence on PET radioligand results.

OpR availability in chronic pain

The positive relationship between OpR availability and recent chronic pain perception could result either from a greater density of OpRs on neuronal cellular membranes (e.g. due to increased trafficking or upregulation), reduced opioid ‘tone’ (reduced release of EOPs resulting in reduced occupation of OpRs), or both. With single scans it is not possible to directly measure opioid tone and OpR density independently. However, opioid ‘tone’ is highly dependent on current pain state, as illustrated by the fact that induction of acute pain

Europe PMC Funders Author Manuscripts

for a short time during PET scanning procedures can be enough to cause a reduction in OpR availability as a result of endogenous opioid release and competitive binding to OpRs [54]. Yet, our data showing a positive association between OpR availability and prior chronic pain perception was statistically independent of intra-scan pain perception. This does not favour the explanation that variability in the concentration of endogenous opioid peptides, released due to intra-scan pain, werecausing the positive correlation between OpR availability and prior chronic pain state.

Our analysis shows that the variances in OpR availability in the caudate nucleus explained by acute pain threshold were present in both chronic pain patients and healthy controls. These variances can therefore be explained by natural variability in OpR density that is independent of the presence of arthritic disease and chronic pain symptoms. A greater density of OpRs would be expected to increase the sensitivity of post-synaptic neurons to opioid-mediated inhibition in response to pain, thereby increasing ‘gain’ in the system.

In animals, delta and kappa-OpRs in the brain and spinal cord were up-regulated in response to mu-OpR agonism [8,11] [56]. For mu-OpRs, there is only evidence of up-regulation in response to *reduced* neurotransmitter binding, just as the normal adaptation to *greater* binding (e.g. in response to morphine [59]) is receptor down-regulation. This may account for the greater anti-nociceptive effects of delta-selective agonists than non-selective agonists in chronic pain states. Together, this evidence implies that delta- and kappa-OpR upregulation would be an expected consequence of chronic pain states. Given that [^{11}C]-DPN is non-selective to OpR subtypes, detection of such an upregulatory response is facilitated and may explain why studies using mu-selective ligands [28] have not detected this mechanism.

Bringing this together, the most likely explanation for our findings is that there is an adaptive upregulation of OpRs in response to chronic pain and that in general greater OpR binding is associated with higher pain threshold and therefore greater pain resilience.

Group differences

The finding of overall lower OpR availability in patients vs. controls may be a result of competition for OpR binding by the release of endogenous ligands as a result of pain being experienced during scanning, and possibly the recycling of receptors as a direct result of this. This finding is consistent with previous studies; reduced OpR availability in the human brain has been associated with rheumatoid arthritis [30], peripheral neuropathic pain [32,39] and fibromyalgia [28]. However, considering these earlier studies, it is surprising that we did not find group differences across more widespread brain regions, with results being restricted to the striatum. It is possible that our study is underpowered to detect differences between groups there are poorly balanced for age and sex. However, patients in our study were also made as comfortable as possible during scanning. The activity-dependent nature of pain in many patients with OA may mean that patients were able to achieve a greater level of comfort inside the scanner that has been possible in patients from these previous studies whose pain is likely to persist when at rest. As shown in Table 1, even though a small number of patients did experience some discomfort that led to higher mean and variance in

intra-scan pain scores in the patient group relative to controls, the ratings are still within the non-painful range.

However, it has been unclear whether findings of lower OpR availability in chronic pain patients compared to pain-free control subjects reflect greater vulnerability to chronic pain states (i.e. reduced OpR density resulting in reduced ability to dampen pain perception via opioidergic inhibition), or are merely a consequence of greater synaptic concentrations of endogenous opioids, released in response to pathological nociception, that compete with the same binding sites as opioid radiotracers. Our findings suggesting upregulation of OpRs in response to chronic arthritic pain clarify that the latter explanation for reductions in OpR availability in chronic pain states is the most likely and that there is increased release of EOPs in chronic arthritic pain.

Striatal mechanisms in chronic pain perception

The striatal dopamine and opioid systems have previously been shown to be abnormal in chronic pain syndromes. Patients with fibromyalgia and orofacial pain syndromes [24,25] have an abnormal dopamine response to pain in the caudate and putamen [57]. Furthermore, there is evidence of increased gray matter density in the striatum in a number of chronic pain conditions including fibromyalgia [50], chronic low back pain [49], and chronic vulvar pain [51]. It is not yet clear how these abnormalities relate to the endogenous opioid system or to pain perception.

Abnormalities in both dopaminergic and opioidergic neurotransmission in the striatum in chronic pain patients might reflect motivational and motor processes such as the learning or expression of conditioned responses to pain [16]. The ventral striatum is a region commonly associated with signalling rewarding outcomes and mediating reinforcement of appetitive behaviour. However, it is also commonly activated during anticipation of pain stimuli [17], particularly the caudate nucleus [47]. Pavlovian prediction learning and evaluation has been associated with the ‘limbic loop’, including the ventral striatum, the basolateral amygdala and the orbitofrontal cortex [10,29]. The nucleus accumbens, in particular, brings evaluative information from the OFC and amygdala to bear on performance by selectively gating information projecting to basal ganglia output nuclei [2,23]. The above networks are involved with the generation of prediction errors for rewarding and aversive stimuli [46,53]. However, prediction error signals in the NAc have been specifically associated with Pavlovian conditioning while prediction errors required for instrumental conditioning involve the putamen [45].

There is also evidence for a relationship between dopamine receptor binding in the ventral striatum (nucleus accumbens) with affective responses to pain [52]. Ventral striatal reward mechanisms may therefore be directly implicated in driving the affective component of pain. However, our data showing a stronger correlation of OpR availability with the sensory than the affective components of pain cast doubt on this hypothesis, and suggest that the ventral striatum may have a more general motivational function in driving behavioural responses to pain. This is consistent with previous work demonstrating that stimulation of the caudate in monkey reduces behavioural reactivity to acute pain [37].

Conclusions

Our data is consistent with an up-regulation of OpRs in response to chronic pain in humans, a hypothesis first identified from animal research and suggested to be part of a homeostatic mechanism that dampens pain perception. This is the first observational evidence consistent with this hypothesis in humans, supported by a correlation between opioid receptor availability and pain resilience (greater pain threshold) in the caudate nucleus. Longitudinal studies are required to identify whether failure to adequately up-regulate OpRs in response to chronic pain may be a risk factor for a more extreme and/or refractory phenotype. Further sequential studies are needed to examine the benefits and pitfalls of current therapeutic approaches to chronic pain in terms of their effects on OpR availability in the brain and the potential for increasing resilience to developing chronic pain from the outset.

Supplementary Material

Refer to Web version on PubMed Central for supplementary material.

Acknowledgements

The study was funded by a project grant from the Medical Research Council (grant reference G0800522) in the United Kingdom. We extend our gratitude to all staff at the Wolfson Molecular Imagine Centre who were essential for the success of this project, in particular: Professor Karl Herholz and Dr Peter Talbot who helped with the initial concept and design, and the radiographers, radiochemists and blood lab for helping to implement the study. We also wish to thank the consultant anaesthetists who aided in the collection of blood data, and especially to our research nurse Ann Lenton who was crucial for patient recruitment.

References

[1]. Aletaha D, Neogi T, Silman AJ, Funovits J, Felson DT, Bingham CO, Birnbaum NS, Burmester GR, Bykerk VP, Cohen MD, Combe B, et al. 2010 Rheumatoid arthritis classification criteria: an American College of Rheumatology/European League Against Rheumatism collaborative initiative. Arthritis Rheum. 2010; 62:2569–81. DOI: 10.1002/art.27584 [PubMed: 20872595]

[2]. Alheid GF, Heimer L. New perspectives in basal forebrain organization of special relevance for neuropsychiatric disorders: the striatopallidal, amygdaloid, and corticopetal components of substantia innominata. Neuroscience. 1988; 27:1–39. [Accessed 11 Apr 2015] [PubMed: 3059226]

[3]. Altman R, Alarcón G, Appelrouth D, Bloch D, Borenstein D, Brandt K, Brown C, Cooke TD, Daniel W, Feldman D, Greenwald R, et al. The American College of Rheumatology criteria for the classification and reporting of osteoarthritis of the hip. Arthritis Rheum. 1991; 34:505–514. DOI: 10.1002/art.1780340502 [PubMed: 2025304]

[4]. Baumgärtner U, Buchholz H-GG, Bellosevich A, Magerl W, Siessmeier T, Rolke R, Höhnemann S, Piel M, Rösch F, Wester H-JJ, Henriksen G, et al. High opiate receptor binding potential in the human lateral pain system. Neuroimage. 2006; 30:692–699. DOI: 10.1016/j.neuroimage.2005.10.033 [PubMed: 16337817]

[5]. Bedson J, Croft PR. The discordance between clinical and radiographic knee osteoarthritis: a systematic search and summary of the literature. BMC Musculoskelet Disord. 2008; 9:116–126. Available: http://www.scopus.com/inward/record.url?eid=2-s2.0-52249116300&partnerID=40&md5=9012f0cc7c66dfa295546dbe5d0bb32f. [PubMed: 18764949]

[6]. Braz JM, Nassar Ma, Wood JN, Basbaum AI. Parallel “pain” pathways arise from subpopulations of primary afferent nociceptor. Neuron. 2005; 47:787–93. DOI: 10.1016/j.neuron.2005.08.015 [PubMed: 16157274]

[7]. Cahill CM, Holdridge SV, Morinville A. Trafficking of delta-opioid receptors and other G-protein-coupled receptors: implications for pain and analgesia. Trends Pharmacol Sci. 2007; 28:23–31. DOI: 10.1016/j.tips.2006.11.003 [PubMed: 17150262]

[8]. Cahill CM, McClellan KA, Morinville A, Hoffert C, Hubatsch D, O'Donnell D, Beaudet A. Immunohistochemical distribution of delta opioid receptors in the rat central nervous system: evidence for somatodendritic labeling and antigen-specific cellular compartmentalization. J Comp Neurol. 2001; 440:65–84. [Accessed 11 Feb 2014] [PubMed: 11745608]

[9]. Cahill CM, Morinville A, Hoffert C, Donnell DO, Beaudet A. Up-regulation and trafficking of d opioid receptor in a model of chronic inflammation: implications for pain control. 2003; 101:199–208.

[10]. Cardinal RN, Parkinson JA, Hall J, Everitt BJ. Emotion and motivation: the role of the amygdala, ventral striatum, and prefrontal cortex. Neurosci Biobehav Rev. 2002; 26:321–52. [Accessed 31 Mar 2015] [PubMed: 12034134]

[11]. Cheng PY, Svingos AL, Wang H, Clarke CL, Jenab S, Beczkowska IW, Inturrisi CE, Pickel VM. Ultrastructural immunolabeling shows prominent presynaptic vesicular localization of delta-opioid receptor within both enkephalin- and nonenkephalin-containing axon terminals in the superficial layers of the rat cervical spinal cord. J Neurosci. 1995; 15:5976–88. [Accessed 11 Feb 2014] [PubMed: 7666182]

[12]. Chudler EH, Dong WK. The role of the basal ganglia in nociception and pain. Pain. 1995; 60:3–38. [Accessed 5 Nov 2013] Available: http://www.sciencedirect.com/science/article/pii/030439599400172B. [PubMed: 7715939]

[13]. Comtat, C.; Sureau, FC.; Sibomana, M.; Hong, IK.; Sjoholm, N.; Trebossen, R. Image based resolution modeling for the HRRT OSEM reconstructions software. 2008 IEEE Nuclear Science Symposium Conference Record; IEEE; 2008. p. 4120-4123.

[14]. Cross AJ, Hille C, Slater P. Subtraction autoradiography of opiate receptor subtypes in human brain. Brain Res. 1987; 418:343–8. [Accessed 5 Nov 2013] [PubMed: 2823963]

[15]. Cunningham VJ, Jones T. Spectral analysis of dynamic PET studies. J Cereb Blood Flow Metab. 1993; 13:15–23. DOI: 10.1038/jcbfm.1993.5 [PubMed: 8417003]

[16]. Daw ND, Shohamy D. The Cognitive Neuroscience of Motivation and Learning. Soc Cogn. 2008; 26:593–620. DOI: 10.1521/soco.2008.26.5.593

[17]. Delgado MR, Li J, Schiller D, Phelps EA. The role of the striatum in aversive learning and aversive prediction errors. Philos Trans R Soc Lond B Biol Sci. 2008; 363:3787–800. DOI: 10.1098/rstb.2008.0161 [PubMed: 18829426]

[18]. Fairclough M, Prenant C, Brown G, McMahon A, Lowe J, Jones A. The automated radiosynthesis and purification of the opioid receptor antagonist, [6-O-methyl-(11) C]diprenorphine on the GE TRACERlab FXFE radiochemistry module. J Labelled Comp Radiopharm. 2014; doi: 10.1002/jlcr.3194

[19]. Fields H. State-dependent opioid control of pain. Nat Rev Neurosci. 2004; 5:565–75. DOI: 10.1038/nrn1431 [PubMed: 15208698]

[20]. Garcia-Larrea L, Peyron R. Pain matrices and neuropathic pain matrices: A review. PAIN®. 2013 [Accessed 31 Oct 2013] Available: http://www.sciencedirect.com/science/article/pii/S0304395913004946.

[21]. Gear RW, Aley KO, Levine JD. Pain-induced analgesia mediated by mesolimbic reward circuits. J Neurosci. 1999; 19:7175–7181. [PubMed: 10436070]

[22]. Gendron L, Lucido AL, Mennicken F, O'Donnell D, Vincent J-P, Stroh T, Beaudet A. Morphine and pain-related stimuli enhance cell surface availability of somatic delta-opioid receptors in rat dorsal root ganglia. J Neurosci. 2006; 26:953–62. DOI: 10.1523/JNEUROSCI.3598-05.2006 [PubMed: 16421315]

[23]. Groenewegen HJ, Wright CI, Beijer AV, Voorn P. Convergence and segregation of ventral striatal inputs and outputs. Ann N Y Acad Sci. 1999; 877:49–63. [Accessed 30 May 2015] [PubMed: 10415642]

[24]. Hagelberg N, Forssell H, Aalto S, Rinne JO, Scheinin H, Taiminen T, Någren K, Eskola O, Jääskeläinen SK. Altered dopamine D2 receptor binding in atypical facial pain. Pain. 2003;

106:43–48. [Accessed 17 Dec 2013] Available: http://www.sciencedirect.com/science/article/pii/S0304395903002756. [PubMed: 14581109]

[25]. Hagelberg N, Forssell H, Rinne JO, Scheinin H, Taiminen T, Aalto S, Luutonen S, Nagren K, Jaaskelainen S. Striatal dopamine D1 and D2 receptors in burning mouth syndrome. Pain. 2003; 101:149–154. Available: ISI:000180588200015. [PubMed: 12507709]

[26]. Hammers A, Allom R, Koepp MJ, Free SL, Myers R, Lemieux L, Mitchell TN, Brooks DJ, Duncan JS. Three-dimensional maximum probability atlas of the human brain, with particular reference to the temporal lobe. Hum Brain Mapp. 2003; 19:224–47. DOI: 10.1002/hbm.10123 [PubMed: 12874777]

[27]. Hammers A, Asselin MC, Turkheimer FE, Hinz R, Osman S, Hotton G, Brooks DJ, Duncan JS, Koepp MJ. Balancing bias, reliability, noise properties and the need for parametric maps in quantitative ligand PET: [(11)C]diprenorphine test-retest data. Neuroimage. 2007; 38:82–94. [PubMed: 17764977]

[28]. Harris RE, Clauw DJ, Scott DJ, McLean SA, Gracely RH, Zubieta JK. Decreased central mu-opioid receptor availability in fibromyalgia. JNeurosci. 2007; 27:10000–10006. [PubMed: 17855614]

[29]. Holland P, Gallagher M. Amygdala circuitry in attentional and representational processes. Trends Cogn Sci. 1999; 3:65–73. [Accessed 30 May 2015] [PubMed: 10234229]

[30]. Jones AK, Cunningham VJ, Ha-Kawa S, Fujiwara T, Luthra SK, Silva S, Derbyshire S, Jones T. Changes in central opioid receptor binding in relation to inflammation and pain in patients with rheumatoid arthritis. Br JRheumatol. 1994; 33:909–916. [PubMed: 7921749]

[31]. Jones AK, Friston K, Dolan R. Positron emission tomography as a research tool in the investigation of psychiatric and psychological disorders. Baillieres ClinEndocrinolMetab. 1991; 5:187–203.

[32]. Jones AK, Kitchen ND, Watabe H, Cunningham VJ, Jones T, Luthra SK, Thomas DG. Measurement of changes in opioid receptor binding in vivo during trigeminal neuralgic pain using [11C] diprenorphine and positron emission tomography. JCerebBloodFlow Metab. 1999; 19:803–808.

[33]. Jones AK, Luthra SK, Pike VW, Herold S, Brady F. New labelled ligand for in-vivo studies of opioid physiology. Lancet. 1985; 2:665–666. [PubMed: 2863651]

[34]. Jones AK, Qi LY, Fujirawa T, Luthra SK, Ashburner J, Bloomfield P, Cunningham VJ, Itoh M, Fukuda H, Jones T. In vivo distribution of opioid receptors in man in relation to the cortical projections of the medial and lateral pain systems measured with positron emission tomography. NeurosciLett. 1991; 126:25–28.

[35]. De Jong HWAM, van Velden FHP, Kloet RW, Buijs FL, Boellaard R, Lammertsma AA. Performance evaluation of the ECAT HRRT: an LSO-LYSO double layer high resolution, high sensitivity scanner. Phys Med Biol. 2007; 52:1505–26. DOI: 10.1088/0031-9155/52/5/019 [PubMed: 17301468]

[36]. Knoess, C.; Rist, J.; Michel, C.; Burbar, Z.; Eriksson, L.; Panin, V.; Byars, L.; Lenox, M.; Wienhard, K.; Heiss, W-D.; Nutt, R. Evaluation of single photon transmission for the HRRT; 2003 IEEE Nuclear Science Symposium. Conference Record; IEEE; 2003. p. 1936-1940.(IEEE Cat. No.03CH37515)

[37]. Lineberry CG, Vierck CJ. Attenuation of pain reactivity by caudate nucleus stimulation in monkeys. Brain Res. 1975; 98:119–134. DOI: 10.1016/0006-8993(75)90513-2 [PubMed: 809117]

[38]. Ma J, Zhang Y, Kalyuzhny AE, Pan ZZ. Emergence of functional delta-opioid receptors induced by long-term treatment with morphine. Mol Pharmacol. 2006; 69:1137–45. DOI: 10.1124/mol.105.019109 [PubMed: 16399848]

[39]. Maarrawi J, Peyron R, Mertens P, Costes N, Magnin M, Sindou M, Laurent B, Garcia-Larrea L. Differential brain opioid receptor availability in central and peripheral neuropathic pain. Pain. 2007; 127:183–194. DOI: 10.1016/j.pain.2006.10.013 [PubMed: 17137714]

[40]. Maes F, Collignon A, Vandermeulen D, Marchal G, Suetens P. Multimodality image registration by maximization of mutual information. IEEE TransMedImaging. 1997; 16:187–98. DOI: 10.1109/42.563664

[41]. Martikainen IK, Peciña M, Love TM, Nuechterlein EB, Cummiford CM, Green CR, Harris RE, Stohler CS, Zubieta J-K. Alterations in endogenous opioid functional measures in chronic back pain. J Neurosci. 2013; 33:14729–37. DOI: 10.1523/JNEUROSCI.1400-13.2013 [PubMed: 24027273]

[42]. Melzack R. The short-form McGill pain questionnaire. Pain. 1987; 30:191–197. Available: http://www.scopus.com/inward/record.url?eid=2-s2.0-0023576853&partnerID=40&md5=31a1300ba77ea4255098d26092611be7. [PubMed: 3670870]

[43]. Meyer RA, Walker RE, Mountcastle VB Jr. A laser stimulator for the study of cutaneous thermal and pain sensations. IEEE TransBiomedEng. 1976; 23:54–60.

[44]. Morinville A, Cahill CM, Esdaile MJ, Aibak H, Collier B, Kieffer BL, Beaudet A. Regulation of delta-opioid receptor trafficking via mu-opioid receptor stimulation: evidence from mu-opioid receptor knock-out mice. J Neurosci. 2003; 23:4888–98. [Accessed 22 Feb 2015] [PubMed: 12832511]

[45]. O'Doherty J, Dayan P, Schultz J, Deichmann R, Friston K, Dolan RJ. Dissociable roles of ventral and dorsal striatum in instrumental conditioning. Science. 2004; 304:452–4. DOI: 10.1126/science.1094285 [PubMed: 15087550]

[46]. O'Doherty JP, Dayan P, Friston K, Critchley H, Dolan RJ. Temporal difference models and reward-related learning in the human brain. Neuron. 2003; 38:329–37. [Accessed 30 May 2015] [PubMed: 12718865]

[47]. Palermo S, Benedetti F, Costa T, Amanzio M. Pain anticipation: An activation likelihood estimation meta-analysis of brain imaging studies. Hum Brain Mapp. 2014; doi: 10.1002/hbm.22727

[48]. Roy M, Shohamy D, Daw N, Jepma M, Wimmer GE, Wager TD. Representation of aversive prediction errors in the human periaqueductal gray. Nat Neurosci. 2014; 17:1607–1612. DOI: 10.1038/nn.3832 [PubMed: 25282614]

[49]. Schmidt-Wilcke T, Leinisch E, Gänßbauer S, Draganski B, Bogdahn U, Altmeppen J, May A. Affective components and intensity of pain correlate with structural differences in gray matter in chronic back pain patients. Pain. 2006; 125:89–97. [Accessed 17 Dec 2013] Available: http://www.sciencedirect.com/science/article/pii/S0304395906002557. [PubMed: 16750298]

[50]. Schmidt-Wilcke T, Luerding R, Weigand T, Jürgens T, Schuierer G, Leinisch E, Bogdahn U. Striatal grey matter increase in patients suffering from fibromyalgia – A voxel-based morphometry study. Pain. 2007; 132:S109–S116. [Accessed 5 Nov 2013] Available: http://www.sciencedirect.com/science/article/pii/S0304395907002679. [PubMed: 17587497]

[51]. Schweinhardt P, Kuchinad A, Pukall CF, Bushnell MC. Increased gray matter density in young women with chronic vulvar pain. Pain. 2008; 140:411–419. [Accessed 17 Dec 2013] Available: http://www.sciencedirect.com/science/article/pii/S0304395908005484. [PubMed: 18930351]

[52]. Scott DJ, Heitzeg MM, Koeppe RA, Stohler CS, Zubieta J-K. Variations in the human pain stress experience mediated by ventral and dorsal basal ganglia dopamine activity. J Neurosci. 2006; 26:10789–95. DOI: 10.1523/JNEUROSCI.2577-06.2006 [PubMed: 17050717]

[53]. Seymour B, Doherty JPO, Dayan P, Koltzenburg M, Jones AK, Dolan RJ, Friston KJ, Frackowiak RS, O'Doherty JP. Temporal difference models describe higher-order learning in humans. Nature. 2004; 429:664–667. [PubMed: 15190354]

[54]. Sprenger T, Valet M, Boecker H, Henriksen G, Spilker ME, Willoch F, Wagner KJ, Wester HJ, To TR, Tolle TR. Opioidergic activation in the medial pain system after heat pain. Pain. 2006; 122:63–67. [PubMed: 16527398]

[55]. Tadokoro M, AKP J, VJ C, D S, S G, J A, T J. Parametric images of [11C]diprenorphine binding using spectral analysis of dynamic PET images acquired in 3D. Ann Nucl Med. 1993; 7:S50–51.

[56]. Wang X-M, Zhou Y, Spangler R, Ho A, Han J-S, Kreek MJ. Acute intermittent morphine increases preprodynorphin and kappa opioid receptor mRNA levels in the rat brain. Mol Brain Res. 1999; 66:184–187. DOI: 10.1016/S0169-328X(99)00021-2 [PubMed: 10095091]

[57]. Wood PB, Schweinhardt P, Jaeger E, Dagher A, Hakyemez H, Rabiner EA, Bushnell MC, Chizh BA. Fibromyalgia patients show an abnormal dopamine response to pain. EurJNeurosci. 2007; 25:3576–3582.

[58]. Woolf AD, Pfleger B. Burden of major musculoskeletal conditions. Bull World Health Organ. 2003; 81:646–656. [PubMed: 14710506]

[59]. Zadina JE, Chang SL, Ge LJ, Kastin AJ. Mu opiate receptor down-regulation by morphine and up-regulation by naloxone in SH-SY5Y human neuroblastoma cells. J Pharmacol Exp Ther. 1993; 265:254–62. [Accessed 5 Nov 2013] [PubMed: 8097244]

[60]. Zubieta J, Smith YR, Bueller JA, Xu Y, Kilbourn MR, Jewett DM, Meyer CR, Koeppe RA, Stohler CS. Regional Mu Opioid Receptor Regulation of Sensory and Affective Dimensions of Pain. 2007:311.

Europe PMC Funders Author Manuscripts

Europe PMC Funders Author Manuscripts

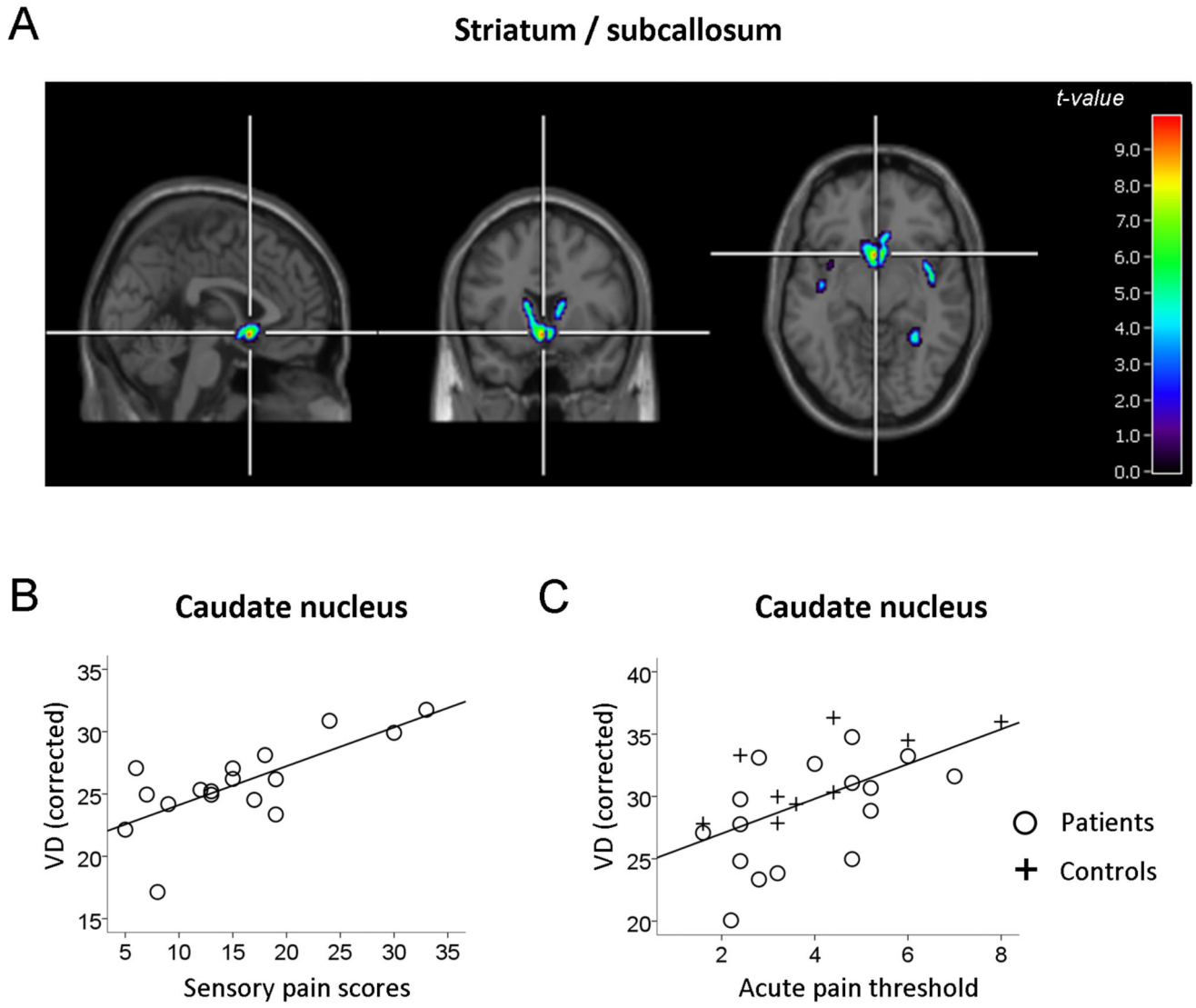

Figure 1. Relationship of ^{11}C-DPN binding to chronic pain perception and acute pain thresholds.

The Volume of Distribution (VD), as a proxy of ^{11}C-DPN binding, was adjusted for a number of nuisance variables in each analysis (see Methods). (a) Whole-brain SPM regression analysis of McGill sensory pain scores as a predictor of ^{11}C-DPN binding (patients only, $n = 17$). Images are displayed at a voxel threshold of $p < 0.001$ uncorrected and a cluster threshold equating to the size of the significant cluster. (b) For illustrative purposes, subsequent extraction of mean VD values from the caudate nucleus was corrected for the same nuisance variables and plotted against McGill sensory pain scores. (c) Pain threshold (laser energy in W cm-2 required to elicit the lowest pain sensation) regressed on VD values (mean across all voxels in the caudate ROI) after correction for nuisance variables. Regression line illustrates fits for the pooled data across groups (patients and controls, $n = 26$).

Europe PMC Funders Author Manuscripts

Table 1

Group characteristics.

Values are means (with standard deviation). Equal variances not assumed. All test are parametric t-tests except for † indicating non-parametric Wilcoxon rank sum test

	***n* total**	***n* females**	**Age (Years)**	**Weight (Kg)**	**DPN dose injected (MBq)**	**H2O dose injected (MBq)**	**Head motion**	**Intra-scan pain ratings**	**Thermal pain threshold (W cm^{-2})**
Arthritis patients	17	12	57.5 (12.1)	83.1 (21.0)	490.0 (62.3)	606.7 (22.3)	3.6 (3.3)	2.5 (2.0)	3.9 (1.5)
Healthy controls	9	3	45.4 (7.5)	78.8 (16.2)	505.0 (33.0)	583.4 (30.7)	1.6 (1.8)	1.5 (1.4)	4.0 (1.9)
Independent samples test p statistic		0.08	*0.004*	0.59	0.26	0.07	0.1456†	0.18	0.76

Europe PMC Funders Author Manuscripts

Table 2

Statistics relating to random and fixed effect analyses on ROIs

Significant effects are italicized. Caud: Caudate Nucleus; Subcal: Subcallosal area; NuAcc: Nucleus Accumbens; Ins: Insula; Puta: Putamen; Thal: Thalamus; ACC: Anterior Cingulate Cortex; PAG: Periaqueductal Gray; r: Pearson's product moment correlation coefficient; p: probability of incorrectly rejecting the null hypothesis.

	McGill sensory pain		**McGill affective pain**		**Acute pain threshold**						**Group**	
	Arthritis patients		***Arthritis patients***		***Groups pooled***		***Arthritis patients***		***Healthy controls***		***Patients vs. controls***	
	r	***p***	***r***	***p***	***r***	***p***	***r***	***p***	***r***	***p***	***t***	***p***
Diprenorphine data												
n	17		17		26		17		9		17, 9	
Caud	0.691	*0.002*	0.587	*0.013*	0.596	*0.002*	0.572	*0.021*	0.735	*0.024*	-2.107	*0.047*
Subcal	0.779	*0.001*	0.536	*0.026*	0.424	*0.035*	0.49	0.054	0.339	0.373	-1.728	0.098
NuAcc	0.691	*0.002*	0.356	0.160	0.300	0.146	0.431	0.096	0.044	0.911	-1.452	0.160
Ins	0.653	*0.003*	0.284	0.269	0.377	0.063	0.454	0.077	0.247	0.521	-1.648	0.113
Puta	0.567	*0.018*	0.197	0.449	0.382	0.060	0.476	0.063	0.204	0.598	-1.770	0.090
Thal	0.601	*0.011*	0.346	0.174	0.301	0.144	0.244	0.363	0.427	0.252	-1.258	0.221
ACC	0.454	0.067	-0.029	0.912	0.135	0.520	0.397	0.128	0.343	0.193	-0.976	0.339
PAG	0.561	*0.019*	-0.030	0.910	0.136	0.516	0.075	0.783	0.275	0.474	-0.445	0.660
Water data												
n	14		14		22		14		8		14, 8	
Caud	0.282	0.329	0.208	0.475	0.524	0.012	0.314	0.274	0.701	0.053	-1.013	0.339